HOKKAIDO UNIVERSITY

Title	Palaeoclimatic evolution and present conditions of the Greenland Ice Sheet in the vicinity of Summit : An approach by large-scale modelling
Author(s)	Greve, R.; Weis, M.; Hutter, K.
Citation	Palaeoclimates : data and modelling, 2(2-3), 133-161
Issue Date	1998
Doc URL	https://hdl.handle.net/2115/34785
Type	journal article
File Information	Greve_etal_1998_Paleoclimates.pdf

Hokkaido University Collection of Scholarly and Academic Papers : HUSCAP

Paleoclimates **2** (2–3), 133–161, 1998
OPA (Overseas Publishers Association) Amsterdam B.V.
— Authors' final version —

Palaeoclimatic evolution and present conditions of the Greenland Ice Sheet in the vicinity of Summit: An approach by large-scale modelling

R. Greve, M. Weis and K. Hutter

Institut für Mechanik, Technische Universität Darmstadt,
D-64289 Darmstadt, Germany

January 15, 1998

Correspondence to: R. Greve (greve@mechanik.tu-darmstadt.de)

Abstract

Using the three-dimensional numerical model SICOPOLIS for polythermal land-based ice sheets in the shallow ice approximation, simulations are performed to determine the velocity, temperature and water-content distributions as well as the evolution of the free surface, the cold-temperate-transition surface (CTS) and the basal surface within the Greenland Ice Sheet through time for a climate driving as determined by the (smoothed) GRIP palaeotemperature record. The model is driven by the temperature at the free surface, the global sea level and the geothermal heat flow 5 km below the basal surface. It uses plausible parameterizations for the accumulation and ablation rates, the basal sliding law and the constitutive behaviour (power-law rheology), in which the fluidity difference between glacial and interglacial ice is accounted for by appropriate enhancement factors.

Computations that cover 250,000 years of climate history are performed with various sets of parameters to find optimal present conditions when compared with available data. To this end a misfit index is defined, and parameterizations are chosen so as to minimize it. It is shown that dating the ice at depth is crucially dependent on the "flux of age" into the base. However, other parameterizations such as the geothermal heat flow or the basal drag in the sliding law etc. equally influence the present geometry of the ice sheet.

We investigate the results of the best-fit simulation with particular attention to the vicinity of Summit, the highest point of the Greenland Ice Sheet at 72° 34′ N, 37° 38′ W, in whose vicinity the two deep ice cores GRIP and GISP2 were drilled. For these boreholes, time series for the ice thickness and the basal temperature, present temperature-depth profiles and present age-depth profiles are presented. Furthermore, the ice-surface topography and the ice thickness in the vicinity of Summit is shown, and a comparison with high-resolution RES data is performed.

Keywords:
Ice sheets, Greenland, GRIP, GISP2, palaeoclimate modelling, dating of ice cores.

1 Introduction

Ice core studies provide interesting and important insight in the Earth's climate history and in the present state of ice sheets. A variety of palaeoclimatic quantities, such as surface temperature, accumulation, composition of the atmosphere etc., can be directly or indirectly inferred from the ice samples, and measurements of temperature, velocity, density, stress, grain size and crystal axes orientation in the borehole characterize the present conditions (Paterson, 1994).

However, there exists a strong interdependence between the interpretation of ice core data and ice sheet modelling. First, dating of the lower parts of the core, where annual variations of the ice composition cannot be resolved and thus stratigraphic techniques fail, must be performed by modelling the dynamic behaviour of the ice sheet at the borehole. Second, paleoclimatic information obtained by interpretation of the ice core data can be used to drive palaeoclimatic simulations of ice sheet dynamics and thermodynamics. Third, data of the present state of the ice sheet may be used to check model results against.

In Greenland, four deep ice cores have been drilled to this day, namely at Camp Century in the northwest, at Dye3 in the south, and recently the two cores GRIP and GISP2 at Summit which provided ice samples reaching back as far as 250,000 years into the past; these cover at least two entire glacial-interglacial cycles. In this study, we use a reconstruction of the surface-temperature and accumulation history from the GRIP core to drive dynamic/thermodynamic simulations for the entire Greenland Ice Sheet with the polythermal ice sheet model SICOPOLIS originally developed by Greve (1995), and focus attention to the model outcome in the vicinity of Summit.

The main objective is to reproduce the present state of the ice sheet, in particular in the Summit region, as accurately as possible in order to support the interpretation of the GRIP and GISP2 cores by providing realistic flow fields and age-depth profiles. Starting from the original set-up by Greve (1995, 1997b), this is achieved by implementing more recent information on boundary conditions such as topography, accumulation and surface melting, and by some adjustment of poorly known physical parameters within their range of plausible values. It is demonstrated that this procedure, indeed, leads to a considerable reduction of the misfit between the measured and the simulated ice sheet. Thus, the computed age-depth profiles at GRIP and GISP2 can be used to complete the dating of these cores in the deeper regions where annual-layer counting is not possible.

The distinctive feature of the model SICOPOLIS is that it accounts for the possible presence of a basal layer of temperate ice (that is, with a temperature at the pressure melting point) in an environment of cold ice (temperature below the pressure melting point). Ice sheets of that kind are referred to as *polythermal*. Therefore, SICOPOLIS computes the temporal evolution of the extent and thickness of the ice sheet as a whole as well as of the basal temperate-ice layer, the velocity field, the temperature field in the cold ice regions, the water content in the temperate ice regions and the age of the ice (the time since its accumulation on the ice surface), driven by the external forcing from surface temperature, surface accumulation (essentially equal to the snowfall rate), sea level and geothermal heat flux from below.

2 Prognostic equations of the model

The computer program SICOPOLIS solves the polythermal ice sheet equations as described by Greve (1995, 1997a). These are based on the continuum-mechanical balance equations and jump conditions of mass, momentum and energy, and the rheology of a density-preserving, heat-conducting power-law fluid with a rate factor strongly dependent on the temperature T and the water content ω,

$$\begin{aligned} \boldsymbol{D} &= EA(T')\, f(\sigma)\, \boldsymbol{t}^{\mathrm{D}} \qquad \text{(cold ice)}, \\ \boldsymbol{D} &= EA_{\mathrm{t}}(\omega)\, f_{\mathrm{t}}(\sigma)\, \boldsymbol{t}^{\mathrm{D}} \qquad \text{(temperate ice)}; \end{aligned} \tag{1}$$

where $\boldsymbol{D}$ is the strain-rate tensor; $\boldsymbol{t}^{\mathrm{D}}$ the stress deviator; E the creep enhancement factor; $A(T')$ the creep rate factor for cold ice, dependent on the homologous temperature $T' = T - T_{\mathrm{melt}}$; $A_{\mathrm{t}}(\omega)$ the creep rate factor for temperate ice; $f(\sigma)$ the creep function for cold ice, $f_{\mathrm{t}}(\sigma)$ the creep function for temperate ice, dependent on the effective shear stress $\sigma = [\mathrm{tr}\,(\boldsymbol{t}^{\mathrm{D}})^2/2]^{1/2}$. The complete set of field equations, boundary and transition conditions is not repeated here; however, the main prognostic equations are listed below. The model equations are subjected to the shallow ice approximation (Hutter, 1983; Morland, 1984), that is, they are scaled with respect to the aspect ratio ε (ratio of typical thickness to typical length), and only lowest-order terms are kept. This entails neglection of acceleration in the momentum balance, so that the velocity field behaves quasi-stationary ("Stokes flow"), and, furthermore, neglection of deviatoric normal stresses.

Ice thickness:

$$\frac{\partial H}{\partial t} = \frac{\partial (h-b)}{\partial t} = -\frac{\partial q_x}{\partial x} - \frac{\partial q_y}{\partial y} + a_{\mathrm{s}}^{\perp} - \frac{\mathcal{P}_{\mathrm{b}}^{\mathrm{w}}}{\rho}; \tag{2}$$

where x, y are the horizontal Cartesian coordinates; z is the vertical Cartesian coordinate (elevation above present sea level); t the time; h the z-coordinate of the ice surface; b the z-coordinate of the ice base or lithosphere surface, respectively; H the ice thickness; q_x, q_y are the components of the horizontal mass flux; $a_{\mathrm{s}}^{\perp}$ is the accumulation-ablation function at the ice surface; $\mathcal{P}_{\mathrm{b}}^{\mathrm{w}}$ the basal melting rate; ρ the density of ice.

Bedrock response to ice load:

$$\frac{\partial b}{\partial t} = -\frac{1}{\tau_{\mathrm{V}}} \left\{ b - \left(b_0 - \frac{\rho}{\rho_{\mathrm{a}}} H \right) \right\}; \tag{3}$$

where τ_{V} is the asthenospheric time lag; b_0 the position b of the relaxed lithosphere surface without ice load; ρ_{a} the density of the asthenosphere.

Temperature (cold ice regions):

$$\frac{\partial T}{\partial t} + v_x \frac{\partial T}{\partial x} + v_y \frac{\partial T}{\partial y} + v_z \frac{\partial T}{\partial z} = \frac{1}{\rho c} \frac{\partial}{\partial z} \left(\kappa \frac{\partial T}{\partial z} \right) + \frac{2}{\rho c} E A(T') f(\sigma) \sigma^2; \tag{4}$$

where v_x, v_y, v_z are the components of the ice velocity; c is the specific heat of ice; κ the heat conductivity of ice.

Water content (temperate ice regions):

$$\frac{\partial \omega}{\partial t} + v_x \frac{\partial \omega}{\partial x} + v_y \frac{\partial \omega}{\partial y} + v_z \frac{\partial \omega}{\partial z} = \frac{2}{\rho L} E A_{\mathrm{t}}(\omega) f_{\mathrm{t}}(\sigma) \sigma^2 - \frac{1}{\rho} D(\omega) + \mathrm{CCC}; \tag{5}$$

where L is the latent heat of ice; $D(\omega)$ the water drainage function; CCC the Clausius-Clapeyron correction (small term, not given explicitly; see Greve, 1995, 1997a).

Age of the ice (cold and temperate ice regions):

$$\frac{\partial \mathcal{A}}{\partial t} + v_x \frac{\partial \mathcal{A}}{\partial x} + v_y \frac{\partial \mathcal{A}}{\partial y} + v_z \frac{\partial \mathcal{A}}{\partial z} = 1 \quad \left(+ D_{\mathrm{A}} \frac{\partial^2 \mathcal{A}}{\partial z^2} \right); \tag{6}$$

where $\mathcal{A}$ is the age of the ice; D_{A} the numerical diffusivity in order to keep the integration stable, see also Huybrechts (1994).

Temperature (lithosphere):

$$\frac{\partial T}{\partial t} + \frac{\partial b}{\partial t} \frac{\partial T}{\partial z} = \frac{\kappa_{\mathrm{r}}}{\rho_{\mathrm{r}} c_{\mathrm{r}}} \frac{\partial^2 T}{\partial z^2}; \tag{7}$$

where κ_{r} is the heat conductivity of the lithosphere; ρ_{r} the density of the lithosphere; c_{r} the specific heat of the lithosphere.

We refrain from discussing the numerical solution technique of SICOPOLIS here. This is done in detail by Greve (1995).

3 Modelling the Greenland Ice Sheet

3.1 Present state of the Greenland Ice Sheet

For all the simulations presented below, the position of the relaxed lithosphere surface without ice load, b_0, must be known. It can be calculated approximately under the assumption that the present lithosphere surface b^{today} is close to equilibrium with the present ice load $H^{\mathrm{today}} = h^{\mathrm{today}} - b^{\mathrm{today}}$,

$$b_0 = b^{\mathrm{today}} + \frac{\rho}{\rho_{\mathrm{a}}} H^{\mathrm{today}}. \tag{8}$$

Hereby, b^{today} and h^{today} are based on data of Letréguilly et al. (1991a). Simulations using different horizontal resolutions were performed. While the 40 km topography data are based on the interpolation by Calov (1994), the 20 km resolution is based on Letréguilly's original data set. Furthermore, for the Summit region high-resolution data on a 2 km grid were inferred from radio echo soundings by Hodge et al. (1990). The measured surface topography h^{today} is shown in Fig. 1.

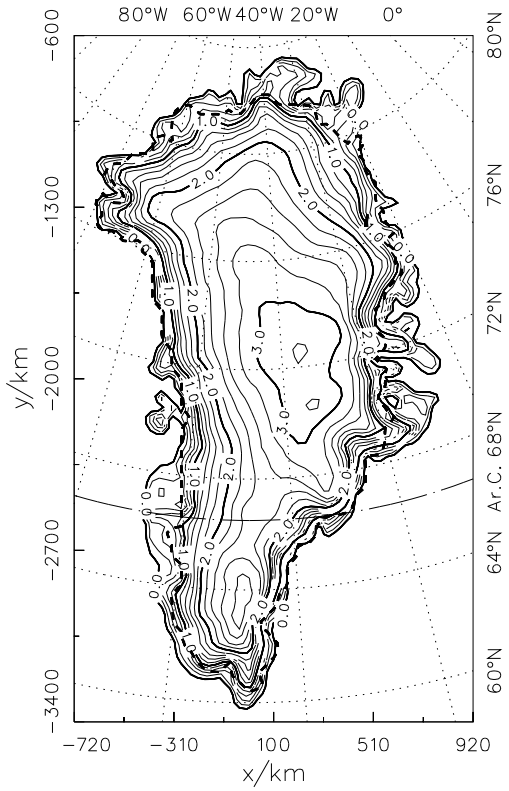

Figure 1: Measured surface topography h^{today} of the present Greenland Ice Sheet, according to Letréguilly et al. (1991) for the whole of Greenland, and Hodge et al. (1990) for the Summit region (in km a.s.l.). The spacing between the isolines is 200 m. The dashed heavy line indicates the ice margin.

The present climate conditions for the ice sheet are characterized by the mean annual air temperature above the ice, T_{ma}, and the accumulation-ablation function, $a_{\text{s}}^{\perp}$ (difference of accumulation rate, S, and surface melting rate, M). As for $T_{\text{ma}}^{\text{today}}$, we use the parameterization given by Reeh (1991) which is based on measurements by Ohmura (1987). The accumulation rate S^{today} applied in our study is based on the data compilation by Ohmura and Reeh (1991), supplemented by recent measurements in the Summit region (Bolzan and Strobel, 1994) and in North Greenland (Wilhelms, 1996). The melting rate M is parameterized by employing the degree-day model (Braithwaite and Olesen, 1989; Reeh, 1991) as implemented by Calov (1994), Calov and Hutter (1996), with different degree-day

factors for the melting of snow, β_{snow}, and for the melting of ice, β_{ice}.

At the lower boundary of the lithosphere layer, the geothermal heat flux is prescribed. Reasonable values cover the range from the value for precambrian shields, $Q^{\perp}_{\mathrm{geoth}} = 42\,\mathrm{mWm}^{-2}$, to the global mean, $Q^{\perp}_{\mathrm{geoth}} = 55\,\mathrm{mWm}^{-2}$ (Lee, 1970).

Finally, calving at the ice-sheet margin is treated implicitly by prescribing a zero ice thickness where the ice reaches the ocean.

3.2 Standard boundary conditions for varying climate scenarios

In order to model the Greenland Ice Sheet under climate conditions different from those at the present, specifications as to how this input varies must also be given. For the mean annual air temperature T_{ma} we assume that the present spatial distribution is preserved; thus, the modification is expressed by a purely time-dependent term. This yields an expression for T_{ma} as a function of geographic latitude ϕ, elevation above present sea level z and time t,

$$T_{\mathrm{ma}}(\phi, z, t) = T_{\mathrm{ma}}^{\mathrm{today}}(\phi, z) + \Delta T_{\mathrm{ma}}(t). \tag{9}$$

For the accumulation rate S, we postulate a linear relation between S and ΔT_{ma} with distinctly reduced accumulation under glacial climate conditions. This yields

$$S(\phi, \lambda, t) = S^{\mathrm{today}}(\phi, \lambda)\left(1 + \gamma\,\Delta T_{\mathrm{ma}}(t)\right) \tag{10}$$

(which only makes sense for $\Delta T_{\mathrm{ma}} > -1/\gamma$, otherwise S becomes negative). Reasonable values for γ are $\gamma = 0.05 \ldots 0.075\,\mathrm{K}^{-1}$, corresponding to a reduction of S by $50\% \ldots 75\%$ for the typical glacial surface temperature $\Delta T_{\mathrm{ma}} = -10°\mathrm{C}$ (Dahl-Jensen et al., 1993; Cutler et al., 1995). In the above relation, S is expressed as a function of geographic latitude ϕ, geographic longitude λ and time t. The connection between the coordinates on the Earth surface ϕ, λ and the model plane x, y is provided by a polar stereographic projection with standard parallel at 71°N.

Eq. (10) comprises the ad-hoc assumption that the present accumulation pattern stays constant throughout the time. Since past accumulation rates cannot be measured, the validity of this assumption could only be confirmed or refuted by atmosphere-ocean modelling. Ohmura et al. (1996) present the result of a GCM ECHAM3 T106 simulation for an expected *future* climate ($2 \times \mathrm{CO}_2$ experiment) and show that this entails a distinct change of the spatial accumulation pattern. On the other hand, precipitation results of different GCMs show a rather large variability, so that reliable accumulation patterns for climates different from today's are not available by now. In this situation, a simple parameterization

like Eq. (10) seems to be a reasonable compromise.

Further, the sea level $z_{\rm sl}$ may deviate from the present level, $z_{\rm sl}^{\rm today} = 0$. This is accounted for by applying a time-dependent sea-level scenario $\Delta z_{\rm sl}(t)$, so that

$$z_{\rm sl}(t) = z_{\rm sl}^{\rm today} + \Delta z_{\rm sl}(t) = \Delta z_{\rm sl}(t). \tag{11}$$

All other parameters are assumed to have the same functional form as for the present state. With these specifications any climate scenario is defined by prescribing the purely time-dependent functions $\Delta T_{\rm ma}(t)$ and $\Delta z_{\rm sl}(t)$.

3.3 Specification of physical quantities

Here the physical quantities used for the simulations are given. These are in detail:

Creep law for cold and temperate ice: Glen's flow law (Paterson, 1994)

$$f(\sigma) = f_{\rm t}(\sigma) = \sigma^{n-1}, \quad \text{with} \quad n = 3. \tag{12}$$

Rate factor for cold ice:
Arrhenius law for $T' < -10°\mathrm{C}$, supplemented by four values in the regime $-10°\mathrm{C} < T' < 0°\mathrm{C}$ (Paterson, 1994),

$$\begin{aligned}
A(T' = 0°\mathrm{C}) &= 3.2 \cdot 10^{-24}\,\mathrm{s^{-1}Pa^{-3}},\\
A(T' = -2°\mathrm{C}) &= 2.4 \cdot 10^{-24}\,\mathrm{s^{-1}Pa^{-3}},\\
A(T' = -5°\mathrm{C}) &= 1.6 \cdot 10^{-24}\,\mathrm{s^{-1}Pa^{-3}},\\
A(T' = -10°\mathrm{C}) &= 0.49 \cdot 10^{-24}\,\mathrm{s^{-1}Pa^{-3}}\\
&\quad \text{(linear interpolation between these values)},\\
A(T') &= A_0\, e^{-Q/R(T_0+T')} \qquad \text{for } T' < -10°\mathrm{C};
\end{aligned} \tag{13}$$

with $T_0 = 273.15\,\mathrm{K}$, the activation energy $Q = 60\,\mathrm{kJ\,mol^{-1}}$, the universal gas constant R, and the coefficient $A_0 = 3.985 \cdot 10^{-13}\,\mathrm{s^{-1}Pa^{-3}}$ which assures a smooth transition of the two regimes.

Rate factor for temperate ice:
According to Lliboutry and Duval (1985) and Paterson (1994),

$$A_{\rm t}(\omega) = A(T' = 0°\mathrm{C}) \cdot (1 + 181.25\,\omega) \tag{14}$$

is a suitable form for this.

Coupling between age and enhancement factor:

$$\begin{array}{lll} E=3 & \text{for } t_{\rm acc} < -132\,\text{kyr} & \text{(pre-Eemian ice)},\\ E=1 & \text{for } -132\,\text{kyr} \le t_{\rm acc} < -114.5\,\text{kyr} & \text{(Eemian ice)},\\ E=3 & \text{for } -114.5\,\text{kyr} \le t_{\rm acc} < -11\,\text{kyr} & \text{(Wisconsin ice)},\\ E=1 & \text{for } t_{\rm acc} \ge -11\,\text{kyr} & \text{(Holocene ice)}; \end{array} \tag{15}$$

with the accumulation time $t_{\rm acc} := t - \mathcal{A}$, denoting the moment when a certain ice particle was deposited on the surface.

Sliding law for cold and temperate ice base:
No-slip and Weertman-type sliding law, respectively:

$$\begin{array}{ll} \boldsymbol{v}_{\rm sl} = \boldsymbol{0} & \text{(cold)},\\ \boldsymbol{v}_{\rm sl} = -\dfrac{C_{\rm sl}}{\rho g}\dfrac{\|\boldsymbol{t}_\parallel\|^p}{(\rho g H)^q}\dfrac{\boldsymbol{t}_\parallel}{\|\boldsymbol{t}_\parallel\|}, \quad \text{with} \quad p=3,\ q=2 & \text{(temperate)}; \end{array} \tag{16}$$

where $C_{\rm sl}$ is the sliding coefficient; $\boldsymbol{t}_\parallel$ the basal shear traction in the bed plane; g the gravity acceleration and $\rho g H$ the overburden pressure. According to Calov (1994), Calov and Hutter (1996), (16) implies

$$\boldsymbol{v}_{\rm sl} = -C_{\rm sl} H\,\|\text{grad}\,h\|^2 \text{grad}\,h \qquad \text{(temperate)}. \tag{17}$$

These authors obtained $C_{\rm sl} = 6\cdot 10^4\,\text{yr}^{-1}$ as a result of flow optimization for present climate conditions.

Water drainage function:
Greve (1995) discussed in detail the introduction of this quantity. A meaningful representation was found to be

$$D(\omega) = \left\{ \begin{array}{ll} 0 & \omega \le \omega_{\rm max} \\ \infty & \omega > \omega_{\rm max} \end{array} \right\} \quad (\text{with } \omega_{\rm max} = 1\%). \tag{18}$$

This is a simple, one-parameter form for $D(\omega)$. $\omega_{\rm max}$ plays the role of a threshold value for the water content in temperate ice, any water surplus is assumed to be instantaneously drained into the ground.

Further quantities are listed in Table 1.

Quantity	**Value**
Density of ice, ρ	$910\,\mathrm{kg\,m^{-3}}$
Density of water, ρ_w	$1000\,\mathrm{kg\,m^{-3}}$
Heat conductivity of ice, κ	$9.828\,e^{-0.0057\,T[\mathrm{K}]}\,\mathrm{W\,m^{-1}K^{-1}}$
Specific heat of ice, c	$(146.3 + 7.253\,T[\mathrm{K}])\,\mathrm{J\,kg^{-1}K^{-1}}$
Latent heat of ice, L	$335\,\mathrm{kJ\,kg^{-1}}$
Clausius-Clapeyron gradient, β	$8.7 \cdot 10^{-4}\,\mathrm{K\,m^{-1}}$
Density $\times$ specific heat of the lithosphere, $\rho_\mathrm{r} c_\mathrm{r}$	$2000\,\mathrm{kJ\,m^{-3}K^{-1}}$
Heat conductivity of the lithosphere, κ_r	$3\,\mathrm{W\,m^{-1}K^{-1}}$
Thickness of the upper lithosphere layer accounted for in the model, H_r	$5\,\mathrm{km}$
Asthenospheric time lag, τ_V	$3000\,\mathrm{yr}$
Density of the asthenosphere, ρ_a	$3300\,\mathrm{kg\,m^{-3}}$
Gravity acceleration, g	$9.81\,\mathrm{m\,s^{-2}}$
Universal gas constant, R	$8.314\,\mathrm{J\,mol^{-1}K^{-1}}$

Table 1: Standard values of physical quantities used for the simulations of this study. For references see Greve (1995).

4 Towards a best large-scale fit

4.1 General remarks

This section aims at providing a simulation which represents the past evolution and the present state of the Greenland Ice Sheet as a whole and of the Summit region as realistically as possible. To this end, we carried out a series of palaeoclimatic simulations, all driven with a surface-temperature history $\Delta T_\mathrm{ma}(t)$ for the last 250,000 years, thus covering the two last glacial-interglacial cycles until today (iteration time $t = -250 \ldots 0\,\mathrm{kyr}$)[1]. It was constructed by converting the original δ^{18}O-vs.-depth data from the GRIP core, which had been dated by counting annual layers back to $t = -14.5\,\mathrm{kyr}$ and applying a steady-state ice flow model beyond this time (Dansgaard et al., 1993), to surface temperatures with the relation given by Johnsen et al. (1992). The resulting driving scenario was subjected to 2000-year smoothing, because otherwise the iterations tended to become unstable at abrupt surface-temperature peaks. The sea-level history $\Delta z_\mathrm{sl}(t)$ was either ignored (runs gp1 – gp3; see below), or a simple, piecewise linear forcing with a glacial minimum of $\Delta z_\mathrm{sl} = -130\,\mathrm{m}$ was applied (runs gp4 – gp9). The forcing functions $\Delta T_\mathrm{ma}(t)$ and $\Delta z_\mathrm{sl}(t)$ are shown in the two uppermost panels of the time-series plot for gp9 (Fig. 4).

[1] Similar simulations were described by Letréguilly et al. (1991b), Huybrechts (1994, 1996), Fabré et al. (1995), Greve (1995, 1997b), Ritz et al. (1996) and Weis et al. (1996).

All simulations were conducted with a horizontal resolution of $\Delta x = \Delta y = 40\,\mathrm{km}$ except for gp9, which is based on a $\Delta x = \Delta y = 20\,\mathrm{km}$ horizontal grid. With the stereographic projection, Greenland lies within the model domain $x \in [-720\,\mathrm{km}, 920\,\mathrm{km}]$, $y \in [-3400\,\mathrm{km}, -600\,\mathrm{km}]$, resulting in 42×71 grid points in the horizontal plane for the 40-km grid, and 83×141 grid points for the 20-km grid. The vertical resolution is 51 grid points in the cold-ice region, and 11 grid points in the temperate-ice region as well as in the lithosphere. The time steps Δt (for Eqs. (2), (3)) and $\widetilde{\Delta t}$ (for Eqs. (4)-(7)) are $\Delta t = 5\,\mathrm{yr}$, $\widetilde{\Delta t} = 100\,\mathrm{yr}$ (runs gp1 – gp3), $\Delta t = 5\,\mathrm{yr}$, $\widetilde{\Delta t} = 50\,\mathrm{yr}$ (runs gp4 – gp8), and $\Delta t = 1\,\mathrm{yr}$, $\widetilde{\Delta t} = 10\,\mathrm{yr}$ (run gp9), respectively. For all simulations, reasonable initial conditions were computed by preceding 100,000-year simulations into the steady-state of the climate conditions at $t = -250\,\mathrm{kyr}$.

In order to obtain a simple quantitative measure for the agreement between the simulated and the measured present Greenland Ice Sheet, we define a *misfit index* J, which includes a variety of ice-sheet parameters for which measurements are at hand:

$$\begin{aligned} J \;=\; & \left(\frac{V_{\mathrm{tot}} - \hat{V}_{\mathrm{tot}}}{\sigma_{V_{\mathrm{tot}}}}\right)^2 + \left(\frac{h_{\mathrm{max}} - \hat{h}_{\mathrm{max}}}{\sigma_{h_{\mathrm{max}}}}\right)^2 + \left(\frac{A_{\mathrm{i,b}} - \hat{A}_{\mathrm{i,b}}}{\sigma_{A_{\mathrm{i,b}}}}\right)^2 \\ & + \left(\frac{d_{\mathrm{GRIP}}}{\sigma_{d_{\mathrm{GRIP}}}}\right)^2 + \left(\frac{H_{\mathrm{GRIP}} - \hat{H}_{\mathrm{GRIP}}}{\sigma_{H_{\mathrm{GRIP}}}}\right)^2 + \left(\frac{\mathcal{A}_{\mathrm{GRIP}} - \hat{\mathcal{A}}_{\mathrm{GRIP}}}{\sigma_{\mathcal{A}_{\mathrm{GRIP}}}}\right)^2 \\ & + \left(\frac{T_{\mathrm{GRIP}} - \hat{T}_{\mathrm{GRIP}}}{\sigma_{T_{\mathrm{GRIP}}}}\right)^2 + \left(\frac{T_{\mathrm{CC}} - \hat{T}_{\mathrm{CC}}}{\sigma_{T_{\mathrm{CC}}}}\right)^2 + \left(\frac{T_{\mathrm{Dye3}} - \hat{T}_{\mathrm{Dye3}}}{\sigma_{T_{\mathrm{Dye3}}}}\right)^2 \\ & + \left(\frac{v_{\mathrm{T4}} - \hat{v}_{\mathrm{T4}}}{\sigma_{v_{\mathrm{T4}}}}\right)^2 + \left(\frac{v_{\mathrm{TA15}} - \hat{v}_{\mathrm{TA15}}}{\sigma_{v_{\mathrm{TA15}}}}\right)^2 + \left(\frac{v_{\mathrm{TA31}} - \hat{v}_{\mathrm{TA31}}}{\sigma_{v_{\mathrm{TA31}}}}\right)^2 ; \end{aligned} \tag{19}$$

with

V_{tot}	total ice volume,
h_{max}	maximum elevation of the ice sheet above present sea level,
$A_{\mathrm{i,b}}$	ice-covered basal area,
d_{GRIP}	distance between the simulated north dome and GRIP (actual north dome),
H_{GRIP}	ice thickness at GRIP,
$\mathcal{A}_{\mathrm{GRIP}}$	age of the basal ice at GRIP,
T_{GRIP}	basal temperature at GRIP,
T_{CC}	basal temperature at Camp Century,
T_{Dye3}	basal temperature at Dye3,
v_{T4}	surface velocity at EGIG station T4 (Carrefour; cf. Hofmann (1974)),
v_{TA15}	surface velocity at EGIG station TA15 (Milcent),
v_{TA31}	surface velocity at EGIG station TA31 (St. Centrale).

Quantities marked with a hat denote data (for values see Table 2), those without a hat simulation results, and the corresponding σ's are standard deviations, chosen such that they represent typical deviations between simulated and measured values as occuring in the several simulations discussed below[2]:

$$\begin{aligned}
\sigma_{V_{\mathrm{tot}}} &= 0.2 \cdot 10^6\,\mathrm{km}^3, & \sigma_{T_{\mathrm{GRIP}}} &= 5\,\mathrm{K},\\
\sigma_{h_{\max}} &= 0.2\,\mathrm{km}, & \sigma_{T_{\mathrm{CC}}} &= 5\,\mathrm{K},\\
\sigma_{A_{\mathrm{i,b}}} &= 0.2 \cdot 10^6\,\mathrm{km}^2, & \sigma_{T_{\mathrm{Dye3}}} &= 20\,\mathrm{K},\\
\sigma_{d_{\mathrm{GRIP}}} &= 100\,\mathrm{km}, & \sigma_{v_{\mathrm{T4}}} &= 20\,\mathrm{m/yr},\\
\sigma_{H_{\mathrm{GRIP}}} &= 0.2\,\mathrm{km}, & \sigma_{v_{\mathrm{TA15}}} &= 10\,\mathrm{m/yr},\\
\sigma_{\mathcal{A}_{\mathrm{GRIP}}} &= 100\,\mathrm{kyr}, & \sigma_{v_{\mathrm{TA31}}} &= 5\,\mathrm{m/yr}.
\end{aligned} \tag{20}$$

These are introduced to make the various contributions to J commensurate; the inverse to these standard deviations can also be interpreted as weighing factors. The reason for the use of squares in Eq. (19) is that this approach corresponds to the L_2-norm which provides the best statistical average.

It turned out that computations using the 20 km horizontal resolution comsume excessive CPU time far too much to be used for all the experiments presented here. Therefore, our strategy is to improve the model using the 40 km topographic data to obtain our best simulation assessed with the misfit index defined above. Then, this best-fit simulation is recomputed with the 20 km resolution.

We are aware that it is not possible to pin down the uncertain physical parameters associated with the dynamics of the Greenland Ice Sheet to a final set of values by this approach. Inverse problems are typically non-unique, and furthermore we do not vary each poorly known parameter. For instance, the value 3000 yr for the asthenospheric time lag τ_{V} (Table 1) is kept constant in all simulations, even though a different value alters the ice-sheet response to rapid climate changes such as the onset of the Eemian and the Holocene interglacial. We wish to emphasize again that the objective of this study is not to solve the inverse problem, but to provide a simulation sufficiently accurate to be applicable to problems of ice-core interpretation.

[2]The influence of T_{Dye3} on J is kept small by choosing a large standard deviation $\sigma_{T_{\mathrm{Dye3}}}$, because the poor agreement of T_{Dye3} for all simulations (Table 2) may be due to a local phenomenon not included in the model (low geothermal heat flux?).

	gp1	gp2	gp3	gp4	gp5	gp6	gp7	gp8	gp9	Data
V_{tot} [10^6 km^3]	3.206	3.081	2.953	2.961	2.968	2.808	2.812	2.859	2.999	2.828
h_{max} [km]	3.468	3.325	3.293	3.299	3.312	3.172	3.162	3.212	3.258	3.233
$A_{\text{i,b}}$ [10^6 km^2]	1.733	1.726	1.709	1.718	1.725	1.677	1.677	1.680	1.745	1.682
d_{GRIP} [km]	50.03	50.03	50.03	56.56	56.56	14.29	14.29	14.29	30.03	0.0
H_{GRIP} [km]	3.088	2.919	2.877	2.908	2.929	2.760	2.834	2.900	3.059	3.029
$\mathcal{A}_{\text{GRIP}}$ [kyr]	104.00	89.34	87.90	88.37	247.33	280.10	286.24	295.68	299.02	250.0
T_{GRIP} [°C]	-15.04	-9.39	-9.35	-9.54	-9.66	-7.17	-6.63	-9.05	-8.93	-8.56
T_{CC} [°C]	-13.51	-10.82	-10.66	-10.13	-10.25	-10.11	-10.03	-10.79	-13.42	-13.0
T_{Dye3} [°C]	-5.91	-4.09	-3.71	-3.43	-3.52	-3.19	-3.19	-3.77	-3.46	-13.22
v_{T4} [m/yr]	131.47	131.29	124.36	119.71	120.28	110.84	111.30	112.82	121.05	102.98
v_{TA15} [m/yr]	55.65	55.21	54.21	53.80	53.56	47.93	47.88	47.94	51.64	47.75
v_{TA31} [m/yr]	17.50	17.53	17.33	17.56	17.33	14.91	14.70	14.68	15.33	14.85
V_{temp} [10^3 km^3]	1.880	1.941	0.264	0.620	0.609	1.039	1.043	0.943	0.418	–
$A_{\text{t,b}}$ [10^6 km^2]	0.530	0.734	0.699	0.712	0.709	0.688	0.685	0.587	0.566	–
J (misfit index)	12.24	8.27	6.23	5.85	3.18	2.84	2.17	1.35	2.43	0.0

Table 2: Data for the present Greenland Ice Sheet; results for simulations gp1 – gp9 as defined in the main text. Simulated values for fixed positions (GRIP, CC, Dye3, T4, TA15, TA31) are computed by averaging the simulated values of the four adjacent grid points, weighed with the inverse distances to these positions.

4.2 Series of palaeoclimatic simulations

4.2.1 Simulation gp1

Our starting point is simulation gp1. Except from a slight adjustment of the rate factors $A(T')$ and $A_t(\omega)$ to the recommendations of Paterson (1994) (Eqs. (13), (14)) and improved choices for the degree-day factor and the glacial accumulation reduction (see third and fourth item below), its set-up is the same as that applied by Greve (1995, 1997b):

- Topography: data of Letréguilly et al. (1991a).
- Present accumulation rate: Calov's (1994) interpolation of the accumulation data listed by Ohmura and Reeh (1991).
- According to Cutler et al. (1995), the accumulation rate during the Last Glacial Maximum 21,000 years ago is more likely to be only about 25% of the present value. Thus, we choose $\gamma = 0.075\,\mathrm{K}^{-1}$, corresponding to a reduction of S by 75% for $\Delta T_{\mathrm{ma}} = -10°\mathrm{C}$.
- Braithwaite (1995) suggests that the degree-day factor β_{ice} is distinctly larger in regions with low summer temperatures (North Greenland) than in regions with high summer temperatures (South Greenland). Therefore, we choose

$$\begin{aligned} &\beta_{\mathrm{ice}}(\phi = 60°\mathrm{N}) = 7\,\tfrac{\mathrm{mm\,WE}}{\mathrm{d\cdot K}}, \\ &\beta_{\mathrm{ice}}(\phi = 80°\mathrm{N}) = 10\,\tfrac{\mathrm{mm\,WE}}{\mathrm{d\cdot K}}, \\ &\text{with linear interpolation for other latitudes } \phi. \end{aligned} \tag{21}$$

- Geothermal heat flux: value for precambrian shields, $Q^{\perp}_{\mathrm{geoth}} = 42\,\mathrm{mWm}^{-2}$.
- No sea-level history applied: $\Delta z_{\mathrm{sl}}(t) \equiv 0$.
- Sliding parameter of Calov (1994): $C_{\mathrm{sl}} = 6 \cdot 10^4\,\mathrm{yr}^{-1}$.
- Numerical basal boundary condition for the age calculation (required because of the artificial diffusion term in (6)): vanishing normal derivative,

$$\left.\frac{\partial \mathcal{A}}{\partial z}\right|_{z=b} = 0. \tag{22}$$

Table 2 lists the results for the present ice sheet ($t = 0$) in terms of the twelve quantities that appear in the definition of the misfit index (Eq. (19)), the volume of temperate ice, V_{temp}, the basal area covered by temperate ice, $A_{\mathrm{i,b}}$, and the misfit index, J. The latter

takes the value $J = 12.24$, revealing the merely moderate quality of this run, owing to the fact that it was originally designed to show the transient behaviour of the ice sheet, and not primarily to fit the present state (Greve, 1995, 1997b). In detail, the simulated ice-sheet volume, V_{tot}, exceeds the value calculated from topography data by 13.4%, the simulated ice-covered basal area, $A_{\mathrm{i,b}}$, the measured value by 3.0%, and the simulated maximum elevation a.s.l., h_{max}, is 235 m too high. Apparently, the ice sheet of gp1 is somewhat too mighty, a fact that is also demonstrated by the three simulated EGIG surface velocities, v_{T4}, v_{TA15} and v_{TA31}, which are distinctly larger than their measured counterparts (by 27.7%, 16.5% and 17.8%, respectively). On the other hand, the simulated basal temperature at the GRIP core position, T_{GRIP}, is 6.5°C below the measured value, and the basal ice there is at least 150 kyr too young.

4.2.2 Simulation gp2

Both the low simulated basal GRIP temperature and the too mighty ice sheet indicate that the precambrian-shield value $Q^{\perp}_{\mathrm{geoth}} = 42\,\mathrm{mWm}^{-2}$ for the geothermal heat flux may be too small. Hence, for simulation gp2, $Q^{\perp}_{\mathrm{geoth}}$ is set at a value close to its global mean, $Q^{\perp}_{\mathrm{geoth}} = 55\,\mathrm{mWm}^{-2}$ (see also Ritz et al. (1996); these authors use the value $Q^{\perp}_{\mathrm{geoth}} = 50\,\mathrm{mWm}^{-2}$ for their best-fit simulation).

As already investigated by Greve and Hutter (1995) for steady-state scenarios, this has a pronounced effect on the ice sheet, in a way that it becomes remarkably thinner and warmer (Table 2), so that the misfit index is reduced to $J = 8.27$. Especially, T_{GRIP} is now very close to the measured value, with a remaining difference of merely 0.83°C. However, V_{tot} and $A_{\mathrm{i,b}}$ are still too large, namely by 8.9% and 2.6%, respectively, and h_{max} is 92 m too high.

4.2.3 Simulation gp3

In order to achieve a further reduction of the ice volume, simulation gp3 was conducted with the settings of gp2; however, the sliding coefficient at the temperate base was increased from $C_{\mathrm{sl}} = 6 \cdot 10^4\,\mathrm{yr}^{-1}$ to $10^5\,\mathrm{yr}^{-1}$. It turns out that this adjustment works in the right direction (Table 2), so that the misfit index is now improved to $J = 6.23$ because of the reductions of V_{tot}, $A_{\mathrm{i,b}}$ and h_{max}, and the better agreement between modelled and measured EGIG surface velocities.

A striking feature of this simulation compared with gp2 is the difference between the modelled volumes of temperate ice, V_{temp} (Table 2). This quantity is more than seven times smaller for gp3 than for gp2, whereas the basal area covered by temperate ice, $A_{\mathrm{t,b}}$ is reduced merely by 4.8%. This is the effect of enhanced downward advection of cold

surface ice due to the intensified sliding in gp3; the great sensitivity of the basal layer of temperate ice to this was already discussed by Greve (1995, 1997b). Unfortunately, no data are at hand for these quantities connected with temperate ice, so that it is not clear which values are more realistic.

4.2.4 Simulation gp4

For simulation gp4, the piecewise linear sea-level scenario (Fig. 4, second panel) was added to the settings of gp3. This does not aim mainly at improving the simulated present ice sheet, but at providing a more realistic evolution of the ice sheet through the climate cycles. Nevertheless, gp4 entails a slight reduction of the misfit index to $J = 5.85$ which is primarily due to the better agreement of the EGIG surface velocities (Table 2). On the other hand, the simulated north dome moved by one grid point to the east in gp4 when compared with gp3, so that the distance from the simulated north dome to the real dome (GRIP position), d_{GRIP}, slightly increased (from 50.03 km to 56.56 km).

4.2.5 Simulation gp5

A large discrepancy, basically unaffected by the previously described changes, is the age of the basal ice at GRIP, $\mathcal{A}_{\mathrm{GRIP}}$. Simulation gp4 provides the value $\mathcal{A}_{\mathrm{GRIP}} = 88.37\,\mathrm{kyr}$, whereas it is estimated to be at least 250 kyr. This discrepancy is due to the fact that the numerical boundary condition (22) prevents the near-basal ice from developing a realistic depth-age gradient (Fig. 2). We remedied this by changing the basal boundary condition according to the following consideration: In the accumulation regions, the depth-age gradient close to the surface is approximately equal to the accumulation rate, S. Due to the ice flow, this layering is strongly thinned towards the base; consequently, the near-basal depth-age gradient is expected to be much smaller than the accumulation rate. Therefore, in simulation gp5 the set-up of gp4 was altered by applying the new basal boundary condition

$$\left.\frac{\partial \mathcal{A}}{\partial z}\right|_{z=b} = -m_{\mathrm{age}} \cdot \frac{1}{S_{\mathrm{mean}}}, \tag{23}$$

where S_{mean} denotes the mean accumulation rate on the ice sheet, and the thinning factor m_{age} can be adjusted such that realistic depth-age profiles are computed. By conducting a series of test runs, we found the value $m_{\mathrm{age}} = 200$ to be suitable.

The effect of this amendment can clearly be seen in Fig. 2, which depicts the computed age-depth profiles at $(x, y) = (200\,\mathrm{km}, -1880\,\mathrm{km})$ (grid point nearest to the actual GRIP position) and $t = 0$ (present Greenland Ice Sheet) for simulations gp5 (new boundary condition) and gp4 (old boundary condition). Whereas the profile of gp4 shows an unrealistic bending towards the abscissa in the near-basal part below approximately 85% depth, the

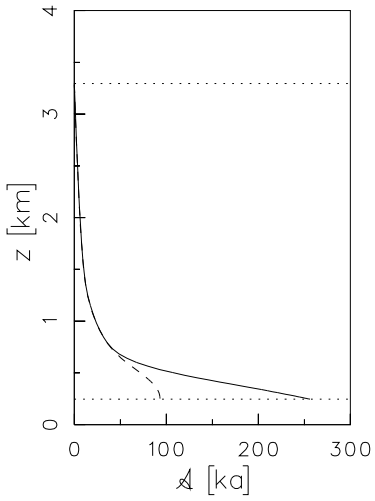

Figure 2: Computed age-depth profiles of the present Greenland Ice Sheet, for the column $(x, y) = (200\,\text{km}, -1880\,\text{km})$ situated nearest to the actual GRIP position. Solid: simulation gp5, with the improved basal boundary condition (23). Dashed: simulation gp4, still with the old boundary condition (22).

profile of gp5 develops a depth-age gradient which is monotonically decreasing with depth, as is expected. As a consequence, the age of the basal GRIP ice, $\mathcal{A}_{\text{GRIP}}$, increased from 88.37 kyr (gp4) to 247.33 kyr (gp5), which is in much better agreement with the estimated value of 250 kyr (Table 2). Thus, the misfit index improved from $J = 5.85$ to $J = 3.18$.

Nevertheless, we are aware that the introduction of the improved boundary condition (23) does not address the primary cause of the problem. As long as the numerical diffusion term in the age equation (6) is retained, it is impossible to really predict the age of the near-basal ice. Future work must consequently aim at avoiding the numerical diffusion by either adopting a stable discretization scheme for the purely advective age equation, or by applying a direct particle-tracing algorithm.

4.2.6 Simulation gp6

Recent accumulation measurements in the Summit region and on the North Greenland Traverse (NGT) of the Alfred Wegener Institute for Polar and Marine Research (Bremerhaven, Germany) provide evidence that the accumulation rates north and northeast of Summit are somewhat smaller than the values inferred from the data of Ohmura and Reeh (1991). Therefore, we constructed a new accumulation map by blanking out the data listed by Ohmura and Reeh (1991) which lie in the Summit region and in the region covered by the NGT, replacing them by the new data (Summit region: Bolzan and Strobel, 1994; NGT region: Wilhelms, 1996), and interpolating the resulting data set on the numerical

grid (Fig. 3).

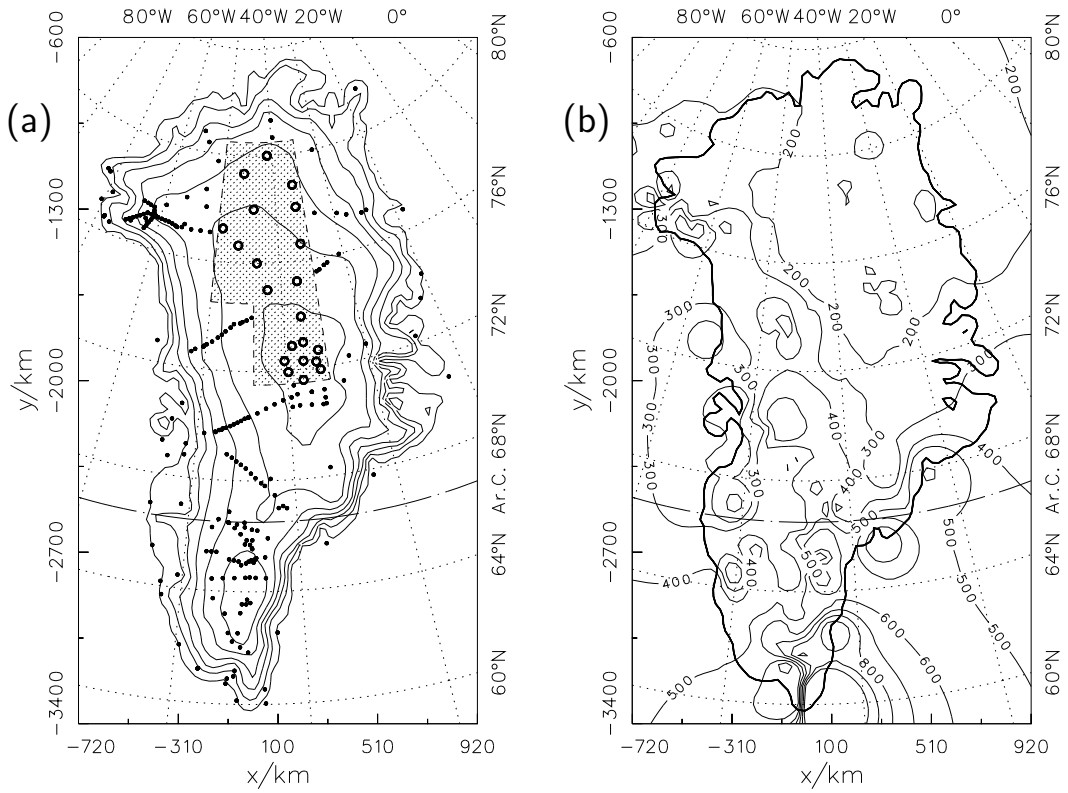

Figure 3: Left (plot a): positions of accumulation measurements listed by Ohmura and Reeh (1991) (small dots) and by Bolzan and Strobel (1994) and Wilhelms (1996) (open circles), on which our new accumulation map, used for simulations gp6 – gp9, is based. The shaded area indicates the region where the data of Ohmura and Reeh are blanked out. Right (plot b): new accumulation map; accumulation rate in mm WE per year (spacing 100 mm WE per year).

For simulation gp6, this updated accumulation map was employed. The most conspicuous effect of this change in model forcing is the improved agreement for the Summit position: d_{GRIP} is reduced from 56.56 km to 14.29 km (Table 2), which represents the optimum agreement possible with the 40 km grid. Together with the EGIG velocities also being distinctly closer to the measured values, this leads to a misfit index of $J = 2.84$.

4.2.7 Simulation gp7

Further, in the Summit region high-resolution topography data (surface, bottom, ice thickness) with a grid spacing of 2 km are available, which cover the region $x \in [120\,\mathrm{km},\ 280\,\mathrm{km}]$, $y \in [-2000\,\mathrm{km},\ -1840\,\mathrm{km}]$ of our model domain (Hodge et al., 1990). Thus, in addition to the settings of gp6, for simulation gp7 we replaced the topography data of Letréguilly et al. (1991a) in this region by the high-resolution data of Hodge et al. (1990) (this does

not mean that a grid refinement was implemented; the grid spacing for the simulation is still 40 km).

Most of the quantities listed in Table 2 are affected only slightly by this alteration. However, due to the better agreement for the thickness of the GRIP column, H_{GRIP}, which reflects the improved bedrock data in the Summit region, the misfit index has dropped to $J = 2.17$.

4.2.8 Simulation gp8

With the changes of simulations gp6 and gp7, the geothermal heat flux $Q^{\perp}_{\mathrm{geoth}} = 55\,\mathrm{mWm}^{-2}$ that was used before is apparently somewhat too large. Further improvement was achieved with the value $Q^{\perp}_{\mathrm{geoth}} = 50\,\mathrm{mWm}^{-2}$, which was therefore applied for simulation gp8.

This provides very good agreement between the simulation and the data. The most conspicuous improvements are that the misfits of V_{tot}, $A_{\mathrm{i,b}}$ and h_{max} are in the range of only 1% (Table 2). A clear amendment is also obvious for the data related with the Summit region. In addition to the improved values of h_{max} and also H_{GRIP}, the basal temperature at GRIP, T_{GRIP}, is now merely 0.5°C too low (Table 2). The misfit index takes the value $J = 1.35$, which represents an enormous improvement when compared with the value 12.24 of our original simulation gp1.

4.2.9 Simulation gp9

This simulation is a repetition of gp8, except for the doubled horizontal resolution (20 km) applied during the period $t = -21\,\mathrm{kyr} \ldots 0\,\mathrm{kyr}$, that is, from the Last Glacial Maximum (LGM) to the present. Compared to gp8, the results for the present ice sheet are non-uniform: while the ice thickness at GRIP, H_{GRIP}, and the basal temperatures at GRIP, T_{GRIP}, and at Camp Century, T_{CC}, are closer to their measured counterparts, the agreement is lesser for the total ice volume, V_{tot}, the ice-covered area, $A_{\mathrm{i,b}}$, the basal temperature at Dye3, T_{Dye3}, the position of the simulated north dome (indicated by d_{GRIP}) and the EGIG surface velocities, v_{T4}, v_{TA15} and v_{TA31} (Table 2). These alterations increase the misfit index to $J = 2.43$. Nevertheless, we regard run gp9 as the best-fit simulation because of the on the whole improved agreement in the vicinity of Summit, and because of the higher resolution of the output data.

The response of the ice sheet to the forcings of air-temperature deviation, ΔT_{ma}, and sea level, z_{sl}, is presented in Fig. 4 as time series of the total ice volume, V_{tot}, the maximum elevation a.s.l., h_{max}, the temperate ice volume, V_{temp}, the maximum thickness of the temperate layer, $H_{\mathrm{t,max}}$, the ice-covered basal area, $A_{\mathrm{i,b}}$ and the basal area covered by temperate ice, $A_{\mathrm{t,b}}$. Evidently, V_{tot} and $A_{\mathrm{i,b}}$ follow the temperature forcing in antiphase,

with a very distinct drop at $t = -127\,\mathrm{kyr}$ (Eemian Ice Volume Minimum, EIVM). This behaviour is due to the enhanced surface melting and the reduced land area liable to glaciation during warm climates. In contrast, the evolution of $h_{\max}$ is in phase with the temperature forcing because the interiour of the ice sheet reacts more sensitively on changes of the accumulation rate which is larger during warm climates (Greve, 1995, 1997b).

As is expected, the quantities concerned with temperate ice, V_{temp}, $H_{\mathrm{t,max}}$ and $A_{\mathrm{t,b}}$, follow the temperature forcing essentially in phase. However, at the EIVM which is characterized by very high air temperatures, the amount of temperate ice is small because of the distinctly reduced ice volume and the consequently reduced strain heating within the ice. It is further noticeable that the present value of V_{temp} is by more than 50% smaller for simulation gp9 than for simulation gp8 (Table 2). This demonstrates the importance of high-resolution computations for the accuracy of predictions of temperate-ice regions.

Figures 5 and 6 show the surface topography and the homologous basal temperature together with the distribution of temperate-ice regions for the three time slices $t = -127\,\mathrm{kyr}$ (EIVM), $t = -21\,\mathrm{kyr}$ (LGM) and $t = 0$ (present), respectively. For the EIVM, in the southwest of the ice sheet a conspicuous narrowing is predicted, that is also paralleled in the north where the ice margin remains far behind the present one. Further, there exists an almost continuous band of basal temperate ice, with three patches of temperate-ice layers in the west, in the east and in the northeast. In contrast, the predicted ice sheet at the LGM is characterized by a glaciated area that covers the entire land surface, with a connection in the northwest via the Canadian Arctic to the Laurentide Ice Sheet (which is not part of the model domain). Some patches of basal temperate ice prevail, but almost no temperate-ice layers are found. The simulated present ice sheet shows a glaciated area in between the extremes of the EIVM and the LGM, the predicted distribution of ice-free regions as well as the surface topography being in good agreement with reality (Fig. 1). Basal temperate ice is found in large near-margin patches, and an extended layer of temperate ice is discernible in Central West Greenland, in coincidence with the occurrence of a very fast ice stream in this area ("Jacobshavns Isbræ").

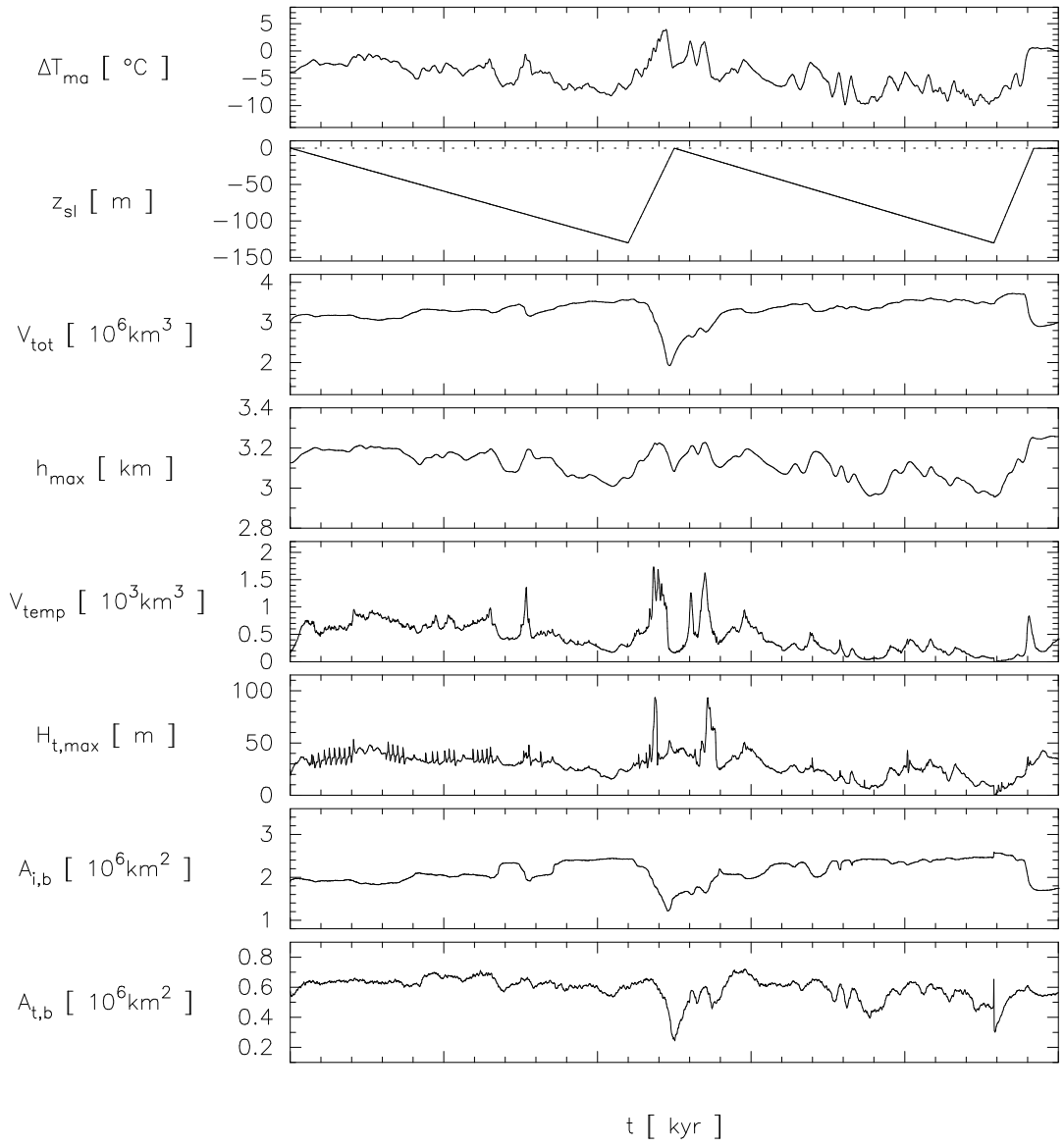

Figure 4: Simulation gp9: model forcings $\Delta T_{\rm ma}$, $z_{\rm sl}$; time evolution of $V_{\rm tot}$, $h_{\rm max}$, $V_{\rm temp}$, $H_{\rm t,max}$, $A_{\rm i,b}$ and $A_{\rm t,b}$ (as defined in the main text).

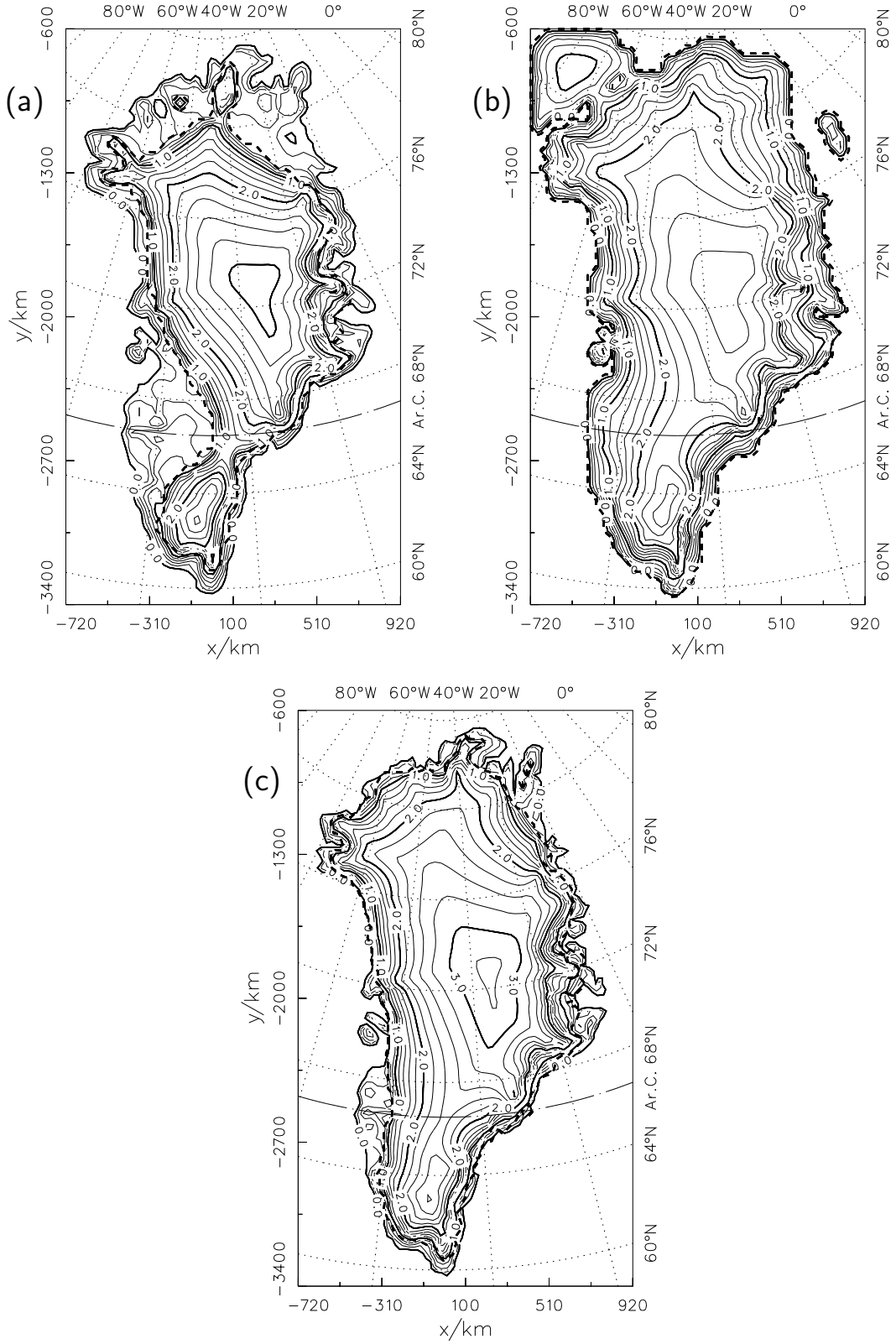

Figure 5: Simulation gp9: surface topography for $t = -127\,\mathrm{kyr}$ (Eemian Ice Volume Minimum, plot a), $t = -21\,\mathrm{kyr}$ (Last Glacial Maximum, plot b) and $t = 0$ (present, plot c), in km a.s.l. The spacing between the isolines is 200 m. The dashed heavy line indicates the ice margin.

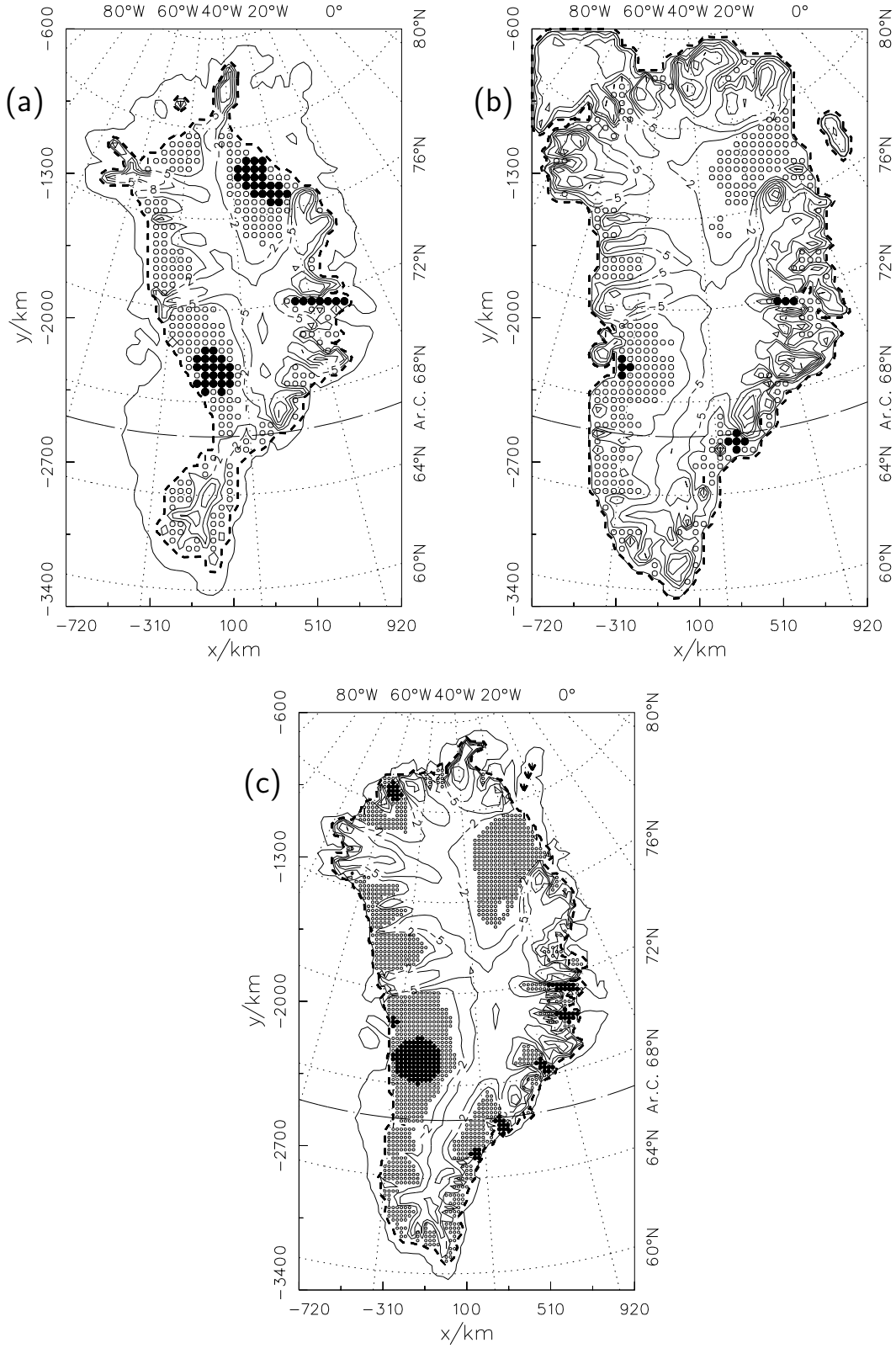

Figure 6: Simulation gp9: homologous temperature at the ice base (in °C), for $t = -127\,\mathrm{kyr}$ (Eemian Ice Volume Minimum, plot a), $t = -21\,\mathrm{kyr}$ (Last Glacial Maximum, plot b) and $t = 0$ (present, plot c). The spacing between the isolines is 3°C. Open circles (full circles) indicate positions where the basal ice is at the pressure melting point with no temperate layer above (with a temperate layer above). The dashed heavy line indicates the ice margin.

5 The vicinity of Summit

The results of run gp9 are now used to investigate the vicinity of Summit, the region where the two deep boreholes GRIP and GISP2 were drilled. Figure 7 depicts the temporal evolution of the mean annual air temperature T_{ma} at GRIP, of the ice thicknesses H at GRIP, H_{GRIP}, and at GISP2, H_{GISP2}, and of the basal temperatures T_{b} at GRIP, T_{GRIP}, and at GISP2, T_{GISP2}. Evidently, H_{GRIP} and H_{GISP2} follow the surface temperature in phase, for the same reasons as h_{max} does (see above). As long as the grid spacing is 40 km (from -250 kyr to the LGM at -21 kyr), the predicted GISP2 column is approximately 100 m thicker than the GRIP column, whereas during the period from the LGM to the present, where 20-km spacing is employed, this difference becomes smaller. The agreement for the present values is very good: the predicted GRIP column is 30 m too thick (3059 m instead of 3029 m), and the predicted GISP2 column is 4 m too thin (3040 m instead of 3044 m). Further, these values are the largest of the entire 250,000 years of model time covered by the simulation.

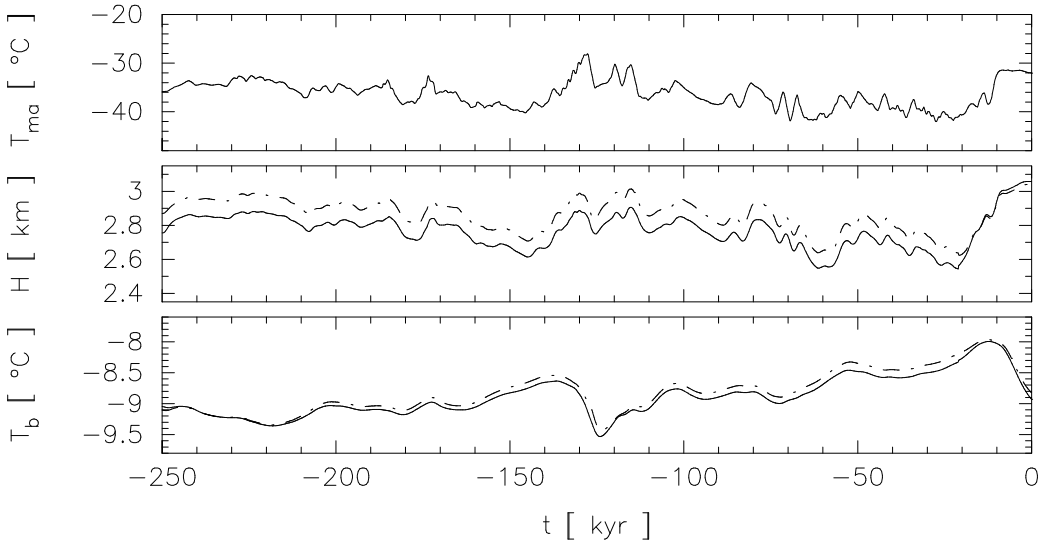

Figure 7: Simulation gp9: time evolution of the mean annual air temperature T_{ma} at GRIP (deduced from the surface temperature forcing, Eq. (9)), the ice thicknesses H at GRIP (solid) and GISP2 (chain-dotted), and the basal temperatures T_{b} at GRIP (solid) and GISP2 (chain-dotted).

As for the basal temperatures, they do not change by more than 1.5°C during the simulation, even though the surface temperatures vary by approximately 14°C. This is due to the impact of the large ice thicknesses in the Summit region, which strongly dampen surface oscillations. Surprisingly, T_{GRIP} and T_{GISP2} are lowest during the warm Eemian, and their values at the LGM exceed today's values. This is so because, during warm climates,

the larger ice velocities enhance advection of cold surface ice towards the base. Since the counteracting effect of enhanced strain heating is not relevant close to ice domes and, consequently, the advection effect is dominant, warm climates entail low basal temperatures around Summit and vice versa. Again, the agreement for the present values is very good: the predicted value for T_{GRIP} is $-8.93°\mathrm{C}$ (measured $-8.56°\mathrm{C}$), the predicted value for T_{GISP2} is $-8.82°\mathrm{C}$ (measured value not yet published).

Figure 8 shows the measured and simulated present surface topographies and ice thicknesses in the vicinity of Summit, where the high resolution RES data by Hodge et al. (1990) are available. Comparing the surface topographies, we see that the shape is reproduced very well in this region, the most conspicuous discrepancy being the region above 3200 m elevation, which is distinctly too large (cf. also Figs. 1 and 5c). Nevertheless, the difference between simulated and measured elevations does nowhere exceed 50 m, and it is even less than 20 m at GRIP and GISP2. The distance between the simulated north dome and GRIP (the actual Summit position) is 30.03 km (Table 2), which is close to the optimum with regard to the 20-km grid. The agreement for the ice thickness distribution is equally convincing. Even though the fine structure of the Hodge data (2 km resolution) cannot be reproduced by the 20-km grid, the main features (almost closed 3200-m isoline in the southwest, 2800-m isoline in the east, general decrease towards the northeast) are very well predicted.

The present temperature and age profiles at GRIP and GISP2 computed by gp9 are shown in Fig. 9. They are compared with the measured temperature profiles (GRIP: Johnsen et al., 1995; GISP2: Cuffey et al., 1995), the GRIP dating by Dansgaard et al. (1993), and the GISP2 dating by Meese et al. (1994) and Sowers et al. (1993) for the last 110 kyr. First, a good agreement for the temperature profiles becomes evident. The maximum differences of 2.5°C occur between 1800 and 2100 m depth, where the ice was accumulated at about the LGM. A possible explanation for this is that the air-temperature reconstruction applied here (see §4.1, first paragraph) may distinctly underestimate the temperature difference between the LGM and the present (Johnsen et al., 1995; Cuffey et al., 1995). Second, the computed age-depth profiles for GRIP and GISP2 are in perfect agreement with the datings for the upper halves of the two cores. In these regions, the datings were produced by counting annual layers and, consequently, are very reliable. This proves that our modelled age-depth profiles are reasonable. At greater depths, gp9 predicts slightly younger ice than the two datings, and very close to the bedrock our predicted ages are distinctly larger (more than 40 kyr for the GRIP core). The discussion in §4.2.6 (see Fig. 2) shows that down to 85% depth the influence of the artificial diffusion term in the age equation (6) has no noteworthy influence on the computed ages. Thus, our results should be reliable down to 85% depth and can be regarded as improvements of previous

datings based on steady-state modelling. However, in the lower parts of the cores the influence of the artificial diffusion term is pronounced, so that the age-depth profile of gp9 is still not suitable for providing precise datings for the lowest 15% of the GRIP and GISP2 cores.

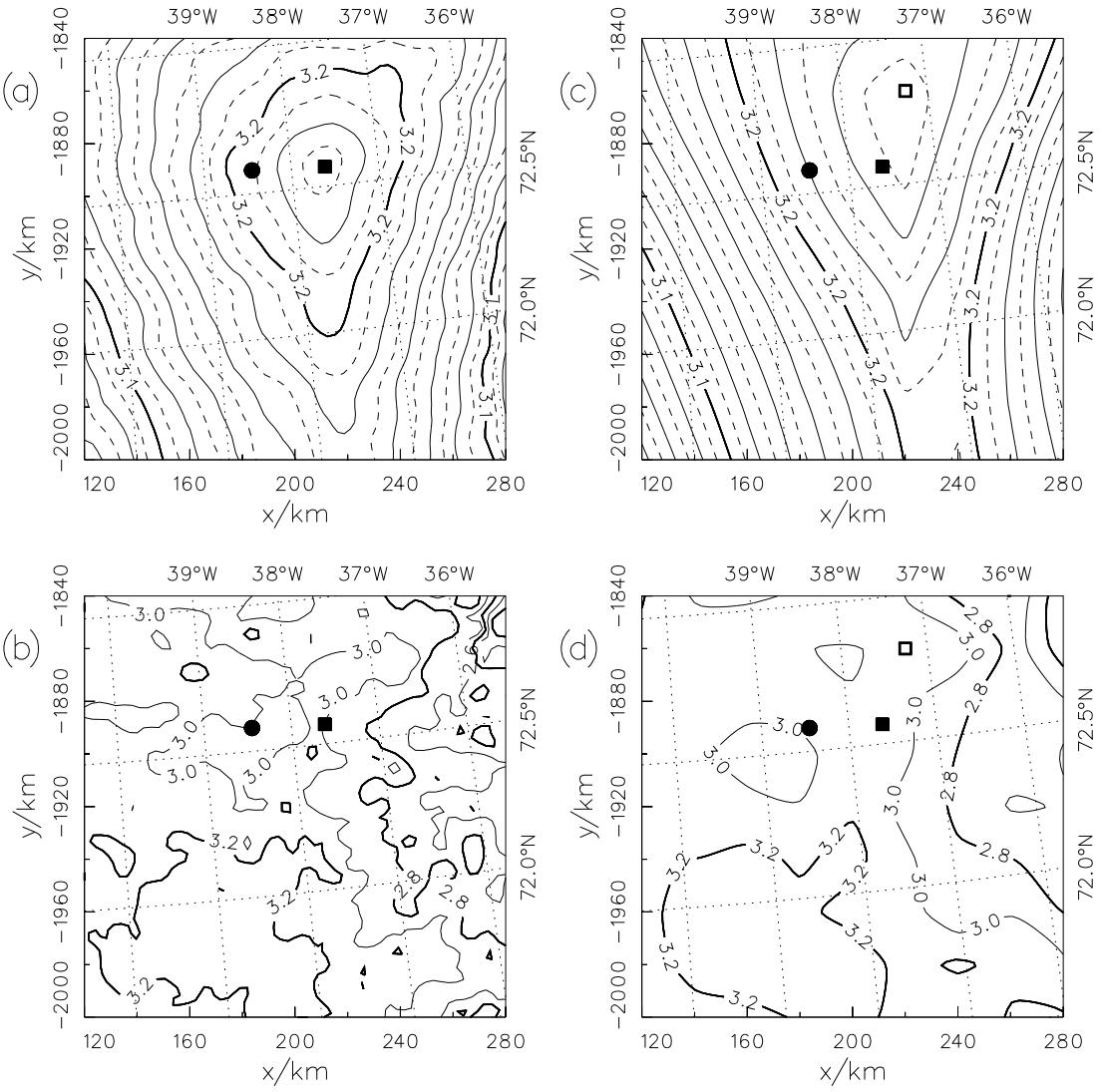

Figure 8: The present vicinity of Summit. Left: measured surface topography (plot a) and ice thickness (plot b), by Hodge et al. (1990). Right: simulated surface topography (plot c) and ice thickness (plot d) from simulation gp9. Full squares show the GRIP position (actual summit), full circles the GISP2 position and open squares the position of the simulated summit (only in panels c, d). Surface elevations are given in km a.s.l. (spacing 10 m), ice thicknesses in km (spacing 200 m).

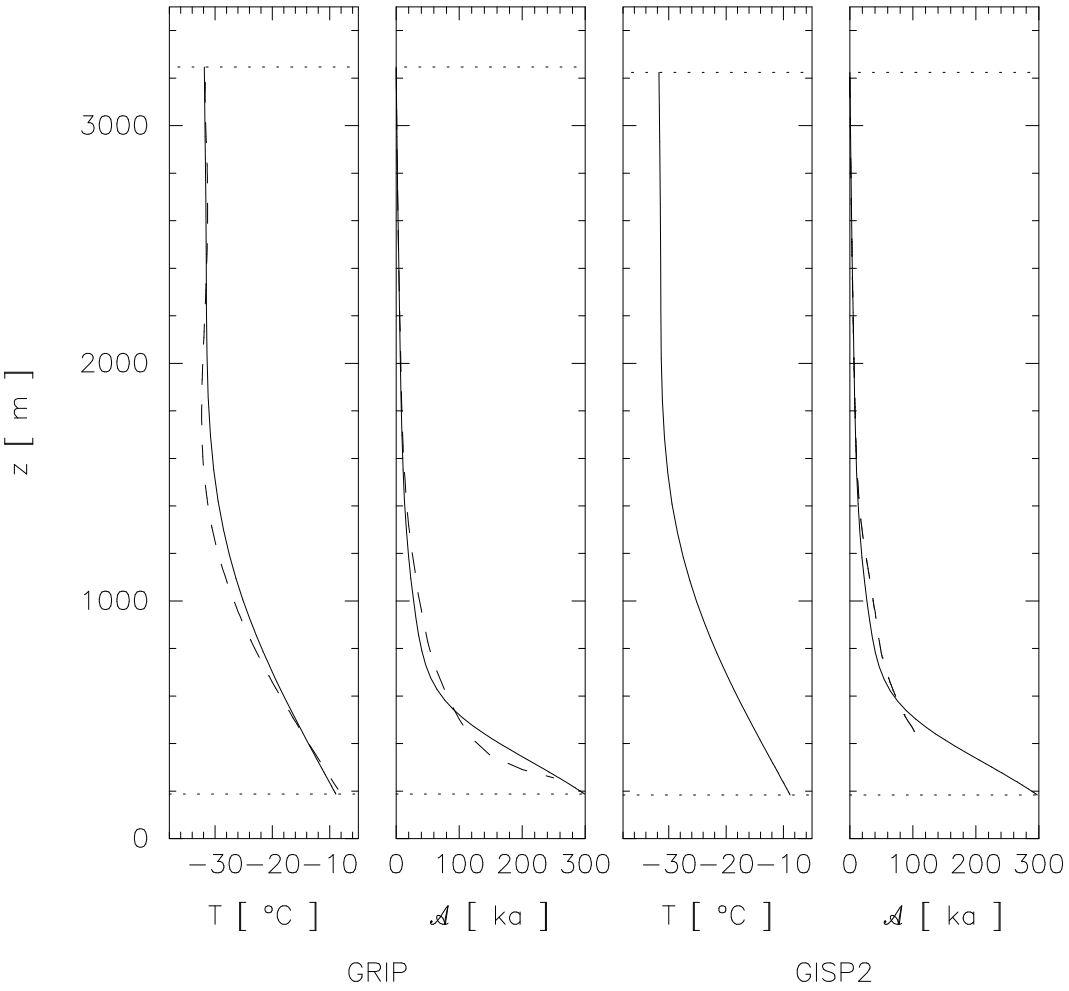

Figure 9: Simulation gp9: present temperature and age profiles for GRIP and GISP2. a) temperature profile for GRIP, together with measured data (by Johnsen et al. (1995); dashed). b) age profile for GRIP, together with the dating by Dansgaard et al. (1993) (dashed). c) temperature profile for GISP2, together with measured data (by Cuffey et al. (1995); dashed). d) age profile for GISP2, together with the dating by Meese et al. (1994), Sowers et al. (1993) (dashed).

6 Conclusion

A series of palaeoclimatic simulations were conducted in order to provide optimum agreement with the present Greenland Ice Sheet as a whole and particularly with the Summit region. The outcome of the so-defined best-fit simulation was used to predict the temporal evolution of the thicknesses and basal temperatures for the two deep ice cores GRIP and GISP2. Further, an intercomparison was carried out with (i) surface-topography and ice-thickness data measured with high spatial resolution in the Summit region, and (ii) borehole temperatures and previous datings of GRIP and GISP2. In all cases, very good agreement was achieved.

Despite these encouraging results, there are still some important aspects of ice-sheet dynamics which have not been accounted for. For increased reliability of simulations of ice dynamics in the neighbourhood of domes, full-scale three-dimensional time-dependent computations ought to be performed with models which replace the presently available models by extending the shallow-ice approximation. This entails incorporation of deviatoric normal stresses, accomodation of induced anisotropy by stress (formation of complex texture) and consideration of topographic variations at the base which presently fall short in the subgrid dimension. Further, the age calculation by the differential equation (6), with the necessity to include some artificial diffusion, should be substituted by particle-tracing algorithms in order to provide unique datings in near-basal layers of ice sheets. Therefore, apart from presenting computational results, our aim was to point out the complexity of the problem and to demonstrate the potential and limitations of the simulation approach.

Acknowledgements

The authors wish to thank Dr. Steve Hodge and Dr. Anne Letréguilly for permission to use their surface-topography and bedrock-topography data of Greenland; Dr. Sigfus Johnsen for providing the δ^{18}O and temperature profiles of the GRIP core; Dr. Georg Bauer for his efforts to keep the institute's workstations operating; Dr. Paul J. Valdes and two anonymous reviewers for their helpful comments on the previous versions of the manuscript.

This work was supported by the Deutsche Forschungsgemeinschaft under project no. Hu 412/14-1.

References

Bolzan, J. F. and M. Strobel. 1994. Accumulation-rate variations around Summit, Greenland. *J. Glaciol.*, **40** (134), 56-66.

Braithwaite, R. J. 1995. Positive degree-day factors for ablation on the Greenland ice sheet studied by energy-balance modelling. *J. Glaciol.*, **41** (137), 153-160.

Braithwaite, R. J. and O. B. Olesen. 1989. Calculation of glacier ablation from air temperature, West Greenland. *Glacier fluctuations and climatic change*, J. Oerlemans (ed.), Kluwer, 219-233.

Calov, R. 1994. Das thermomechanische Verhalten des grönländischen Eisschildes unter der Wirkung verschiedener Klimaszenarien – Antworten eines theoretisch-numerischen Modells. Ph. D. thesis, Institut für Mechanik, Technische Universität Darmstadt, Germany, 171 pp.

Calov, R. and K. Hutter. 1996. The thermomechanical response of the Greenland ice sheet to various climate scenarios. *Climate Dynamics*, **12**, 243-260.

Cuffey, K. M., G. D. Clow, R. B. Alley, M. Stuiver, E. D. Waddington and R. W. Saltus. 1995. Large Arctic temperature change at the Wisconsin-Holocene glacial transition. *Science*, **270**, 455-458.

Cutler, N. N., C. F. Raymond, E. D. Waddington, D. A. Meese and R. B. Alley. 1995. The effect of ice-sheet thickness change on the accumulation history inferred from GISP2 layer thicknesses. *Ann. Glaciol.*, **21**, 26-32.

Dahl-Jensen, D., S. J. Johnsen, C. U. Hammer, H. B. Clausen and J. Jouzel. 1993. Past accumulation rates derived from observed annual layers in the GRIP ice core from Summit, Central Greenland. *Ice in the Climate System*, W. R. Peltier (ed.), Springer-Verlag Berlin etc., 517-532.

Dansgaard, W., S. J. Johnsen, H. B. Clausen, D. Dahl-Jensen, N. S. Gundestrup, C. U. Hammer, C. S. Hvidberg, J. P. Steffensen, A. E. Sveinbjörnsdottir, J. Jouzel and G. Bond. 1993. Evidence for general instability of past climate from a 250-kyr ice-core record. *Nature*, **364**, 218-220.

Fabré, A., A. Letréguilly, C. Ritz and A. Mangeney. 1995. Greenland under changing climates: sensitivity experiments with a new three-dimensional ice sheet model. *Ann. Glaciol.*, **21**, 1-7.

Greve, R. 1995. *Thermomechanisches Verhalten polythermer Eisschilde – Theorie, Analytik, Numerik*. Doctoral thesis, Institut für Mechanik, Technische Universität Darmstadt, Germany, 226 pp. Shaker Verlag (Series "Berichte aus der Geowissenschaft"), Aachen, Germany. ISBN: 3-8265-0999-4.

Greve, R. 1997a. A continuum-mechanical formulation for shallow polythermal ice sheets. *Phil. Trans. R. Soc. Lond.*, A **355**, 921-974.

Greve, R. 1997b. Application of a polythermal three-dimensional ice sheet model to the Greenland Ice Sheet: Response to steady-state and transient climate scenarios. *J. Climate*, **10** (5), 901-918.

Greve, R. and K. Hutter. 1995. Polythermal three-dimensional modelling of the Greenland ice sheet with varied geothermal heat flux. *Ann. Glaciol.*, **21**, 8-12.

Hodge, S. M., D. L. Wright, J. A. Bradley, R. W. Jacobel, N. Skou and B. Vaughn. 1990. Determination of the surface and bed topography in Central Greenland. *J. Glaciol.*, **36** (122), 17-30.

Hofmann, W. 1974. Die Internationale Glaziologische Grönland-Expedition EGIG. *Z. Gletscherkd. Glazialgeol.*, **5**, 217-224.

Hutter, K. 1983. *Theoretical glaciology; material science of ice and the mechanics of glaciers and ice sheets.* D. Reidel Publishing Company, Dordrecht, Holland, 510 pp.

Huybrechts, P. 1994. The present evolution of the Greenland ice sheet: an assessment by modelling. *Global Planet. Change*, **9**, 39-51.

Huybrechts, P. 1996. Basal temperature conditions of the Greenland ice sheet during the glacial cycles. *Ann. Glaciol.*, **23**, 226-236.

Johnsen, S. J., H. B. Clausen, W. Dansgaard, K. Fuhrer, N. Gundestrup, C. U. Hammer, P. Iversen, J. Jouzel, B. Stauffer and J. P. Steffensen. 1992. Irregular glacial interstadials recorded in a new Greenland ice core. *Nature*, **359**, 311-313.

Johnsen, S. J., D. Dahl-Jensen, W. Dansgaard and N. Gundestrup. 1995. Greenland palaeotemperatures derived from GRIP borehole temperature and ice core isotope profiles. *Tellus*, **47B**, 624-629.

Lee, W. H. K. 1970. On the global variations of terrestrial heat flow. *Phys. Earth Planet. Inter.*, **2** (5), 332-341.

Letréguilly, A., P. Huybrechts and N. Reeh. 1991a. Steady-state characteristics of the Greenland Ice Sheet under different climates. *J. Glaciol.* **37** (125), 149-157.

Letréguilly, A., N. Reeh and P. Huybrechts. 1991b. The Greenland ice sheet through the last glacial-interglacial cycle. *Palaeogeogr., Palaeoclimatol., Palaeoecol. (Global Planet. Change Sect.)*, **90**, 385-394.

Lliboutry, L. and P. Duval. 1985. Various isotropic and anisotropic ices found in glaciers and polar ice caps and their corresponding rheologies. *Ann. Geophys.*, **3** (2), 207-224.

Meese, D., R. Alley, T. Gow, P. M. Grootes, P. Mayewski, M. Ram, K. Taylor, E. Waddington and G. Zielinski. 1994. Preliminary depth-age scale of the GISP2 ice core. CRREL Special Report 94-1.

Morland, L. W. 1984. Thermo-mechanical balances of ice sheet flows. *J. Geophys. Astrophys. Fluid Dyn.*, **29**, 237-266.

Ohmura, A. 1987. New temperature distribution maps for Greenland. *Z. Gletscherkd. Glazialgeol.*, **23**, 1-45.

Ohmura, A. and N. Reeh. 1991. New precipitation and accumulation maps for Greenland. *J. Glaciol.*, **37**, 140-148.

Ohmura, A., M. Wild and L. Bengtsson. 1996. Present and future mass balance of the ice sheets simulated with GCM. *Ann. Glaciol.*, **23**, 187-193.

Paterson, W. S. B. 1994. *The physics of glaciers*. 3rd ed. Oxford etc., Pergamon Press, 480 pp.

Reeh, N. 1991. Parameterization of melt rate and surface temperature on the Greenland Ice Sheet. *Polarforschung*, **59** (3), 113-128.

Ritz, C., A. Fabré and A. Letréguilly. 1996. Can an ice sheet model simulate the present Greenland ice sheet? Consequences on the evolution through the last climatic cycle. Preprint, Laboratoire de Glaciologie et Géophysique de l'Environnement, CNRS, Saint Martin d'Hères Cedex, France.

Sowers, T., M. Bender, L. Labeyrie, D. Martinson, J. Jouzel, D. Raynaud, J. J. Pichon and Y. Korotkevich. 1993. 135,000 year Vostok-SPECMAP common temporal framework. *Paleoceanography*, **8**, 737-766.

Weis, M., K. Hutter and R. Calov. 1996. 250,000 years in history of the Greenland Ice Sheet. *Ann. Glaciol.*, **23**, 359-363.

Wilhelms, F. 1996. Leitfähigkeits- und Dichtemessung an Eisbohrkernen. *Ber. Polarforschung*, **191**, 224 pp.